Selection and control of pathways by using externally adjustable noise on a stochastic cubic autocatalytic chemical system

Jean-Sébastien Gagnon,[1,2,*] David Hochberg,[3,†] and Juan Pérez-Mercader[1,4,‡]
[1]*Department of Earth and Planetary Sciences, Harvard University, Cambridge, Massachusetts 02138, USA*
[2]*Natural Sciences Department, Castleton University, Castleton, Vermont 05735, USA*
[3]*Department of Molecular Evolution, Centro de Astrobiología (CSIC-INTA), Torrejón de Ardóz, Madrid, Spain*
[4]*Santa Fe Institute, Santa Fe, New Mexico 87501, USA*

(Received 20 February 2018; revised manuscript received 20 November 2018; published 20 December 2018)

We investigate the effect of noisy feed rates on the behavior of a cubic autocatalytic chemical reaction model. By combining the renormalization group and stoichiometric network analysis, we demonstrate how externally adjustable random perturbations (extrinsic noise) can be used to select reaction pathways and therefore control reaction yields. This method is general and provides the means to explore the impact that changing statistical parameters in a noisy external environment (such as noisy feed rates and fluctuating reaction rates induced by noisy light) has on chemical fluxes and pathways, thus demonstrating how external noise may be used to control, promote, direct, and optimize chemical progress through a given reaction pathway.

DOI: 10.1103/PhysRevE.98.062216

I. INTRODUCTION

It is well known that fluctuations and noise can affect the behavior of various systems, from running coupling constants in high-energy particle physics (e.g., [1]) to phase transitions in condensed matter physics (e.g., [2]) and noise-induced transitions in complex systems (e.g., [3,4]). In particular, noise can affect the dynamics of chemical reactions. For example, it has been shown that external mechanical noise (shaking vs stirring) changes the output of chemical replicator reactions [5] and that coherence resonance can be induced in the Belousov-Zhabotinsky (BZ) reaction by external colored noise [6,7].

Systems undergoing chemical reactions offer a promising and fertile field where selection effects due to external noise can be tested, observed, and refined for specific purposes in mind. The realm of complex chemical phenomena that could be manipulated and controlled in this way with external noise includes sustained chemical oscillations [6–9], pattern formation [10,11], excitable dynamics and front propagation [12–15], or any nonlinear chemical systems where the number of constituents is sufficiently large so as to allow smooth concentrations to be defined [16].

The purpose of this paper is to demonstrate how external experimentally adjustable noise can be used to control and *select* chemical pathways [17]. By adjustable noise we mean any external condition on a chemical system (feed rate, illumination, etc.) that can be varied in a stochastic manner, and for which the statistical properties (amplitude, spectral exponent, etc.) can be varied experimentally. Applying light to the photosensitive dioxide-iodine-malonic acid reaction in order to induce the disappearance of Turing structures is only one example of the above [18]. These stochastic variations in external conditions induce fluctuations in the chemical concentrations, which manifest as noise-dependent modifications of the chemical kinetics. We illustrate our method using a cubic autocatalytic reaction subjected to a noisy feed rate with Gaussian power-law statistics, but the method developed here is general and can be applied to other chemical systems subjected to other types of noise.

To demonstrate how chemical pathways can be selected using noise, we combine stoichiometric network analysis (SNA) with the dynamic renormalization group (RG). SNA is a powerful algebraic method used to study both the dynamics and stationarity properties of chemical reactions [19–21]. The pathway architecture and topology of any chemical reaction network can be elucidated using SNA. The method is based on convex analysis [22], and determines a unique set of extreme currents or extreme flux modes (EFMs) which correspond to the edges of a convex polyhedral flux cone in a Euclidean reaction-rate space. Following this algebraic technique, all possible stationary fluxes are then represented by positive linear combinations of these cone edge vectors. SNA furnishes an efficient method for determining the stability of nonequilibrium steady states by focusing on the behavior of steady-state reaction rates, their associated matter fluxes, chemical pathways, and the extreme currents involving the major subnetworks of the overall chemical mechanism.

The renormalization group allows us to compute and express the effect of fluctuations operating at shorter or longer scales on a system as a nontrivial rescaling of the parameters of the system. For chemical reactions, those parameters are typically the decay rates (r) and reaction rates (λ). In the context of SNA, the important parameters characterizing the dynamics of the reaction (i.e., which chemical pathway is predominant) are the inverse stationary concentrations (h) and the convex parameters (j). These latter parameters represent

*gagnon01@fas.harvard.edu
†hochbergd@cab.inta-csic.es
‡jperezmercader@fas.harvard.edu

the strength of the matter fluxes traversing a specific chemical pathway. Noise affects both (h, j), and the renormalization group allows us to compute their scaling (or "running") as a function of the properties of the noise [23–27]. Thus the use of the RG, taken as input for SNA, enables us to establish a direct link between noise properties and the predominant chemical pathways traversed by the noise-perturbed network of reactions. In other words, if one or more of the model parameters (r, λ) run with scale (where the running is controlled by the noise parameters), this will affect the strengths of the chemical fluxes (j) traversing the pathways, and we then have evidence of noise-controlled fluxes.

II. THEORETICAL METHOD

A. Deterministic CAR model

To illustrate our method, we consider a simple well-known spatially homogeneous cubic autocatalytic reaction (CAR) model (e.g., [28,29]). The model has an interesting and rich phenomenology when spatially heterogeneous states (rather than only well-stirred, homogeneous states) are considered. Indeed, simulations of the deterministic [30] and stochastic [10] versions of this reaction-diffusion model reveal the appearance of a variety of patterns such as stripes, spirals, and self-replicating domains. Due to its autocatalytic nature and the appearance of self-replicating structures, this model is often taken as an extremely primitive form of proto-metabolism.

The CAR model involves the following reactions [29]:

$$U + 2V \xrightarrow{\lambda} 3V, \tag{1}$$

$$V \xrightarrow{r_v} P, \tag{2}$$

$$U \xrightarrow{r_u} Q, \tag{3}$$

$$\xrightarrow{f} U. \tag{4}$$

A substrate U, viewed as the "nutrient" in the living system interpretation of this model, is fed into the system at a constant rate f. The species V, viewed as the "organism," consumes the substrate U and converts it into a copy of V via a second-order autocatalytic reaction with rate constant λ. This autocatalytic reaction embodies a crude form of proto-metabolism. In numerical simulations in spatially extended systems, the species V forms cell-like domains over the substrate U in a certain parameter range [10,30–32]. Both species V and U decay into inert products P and Q with decay rates r_v and r_u, respectively. In a well-stirred system, the deterministic evolution equations corresponding to reactions (1)–(4) are

$$\frac{dV(t)}{dt} = -r_v V(t) + \lambda U(t) V^2(t), \tag{5}$$

$$\frac{dU(t)}{dt} = -r_u U(t) - \lambda U(t) V^2(t) + f, \tag{6}$$

where $V(t)$ and $U(t)$ represent the time-dependent concentrations of species V and U.

B. Stoichiometric network analysis of the CAR model

The stoichiometric network analysis of the CAR model results as follows (see Appendix A for a concise introduction to SNA). The stoichiometric matrix and extreme flux modes corresponding to the four reactions (1)–(4) are given by

$$\boldsymbol{S} = \begin{bmatrix} -1 & 0 & -1 & 1 \\ 1 & -1 & 0 & 0 \end{bmatrix}, \tag{7}$$

$$\boldsymbol{E}_1 = (0, 0, 1, 1), \quad \boldsymbol{E}_2 = (1, 1, 0, 1). \tag{8}$$

These EFMs satisfy $\boldsymbol{S} \cdot \boldsymbol{E}_{1,2} = \boldsymbol{0}$, and belong to the intersection of the right null space of $\boldsymbol{S}$ with the positive orthant R^4_+. These extreme fluxes involve the two elementary chemical pathways of reactions (1)–(4). These are made explicit in Table I and schematically shown in Fig. 1. A general stationary reaction rate vector $\boldsymbol{v}$, for the four reactions, is represented as a point in R^4_+, and is expressed as a positive linear combination of these EFMs:

$$\boldsymbol{v} = j_1 \boldsymbol{E}_1 + j_2 \boldsymbol{E}_2 = (j_2, j_2, j_1, j_1 + j_2). \tag{9}$$

The expansion coefficients $j_i > 0$ are the convex parameters, and correspond to the *magnitudes of the matter fluxes* along the specific reaction pathway represented by $\boldsymbol{E}_i$. As we demonstrate below, these fluxes can undergo *renormalization* due to external noise. From Eqs. (1)–(4) we write the individual stationary-state (ss) reaction rates as a four-component vector:

$$\boldsymbol{v} = \left(\lambda [U]_{ss} [V]^2_{ss}, r_v [V]_{ss}, r_u [U]_{ss}, f\right). \tag{10}$$

TABLE I. Elementary flux modes (EFMs) for the well-mixed CAR model [see Eqs. (1)–(4)] and their corresponding reaction pathways and internal species. The magnitude of the matter flux along each pathway is given by the corresponding convex parameter: $j_1 > 0$, $j_2 > 0$; see Eq. (9).

EFM	Reactions	Pathway	Internal species	Net reaction
$\boldsymbol{E}_1$	(4)	$f \to U$	U	$f \to Q$
	(3)	$U \to Q$		
$\boldsymbol{E}_2$	(4)	$f \to U$	V, U	$f \to P$
	(1)	$U + 2V \to 3V$		
	(2)	$V \to P$		

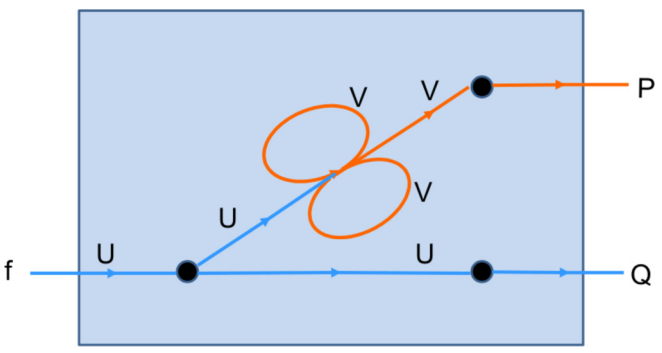

FIG. 1. The two reaction pathways of the CAR model (see also Table I). The bounding box encloses a well-mixed system with input and output flows maintaining the reactions out of equilibrium. The lower pathway (blue) involves reactions (4) and (3), while the upper pathway (orange) involves the reactions (4), (1), and (2); see Table I for details. An observer *external* to the enclosure detects only the net transformations $f \to Q$ and $f \to P$.

Equating the above two stationary-state vectors (9) and (10) and introducing the stationary inverse concentrations h_1, h_2 (where $h_1 = h_u = 1/[U]_{ss}$ and $h_2 = h_v = 1/[V]_{ss}$) implies

$$\lambda = j_2 h_u h_v^2, \quad r_v = j_2 h_v, \quad r_u = j_1 h_u, \quad f = j_1 + j_2. \tag{11}$$

Below we use the above identities to deduce the scale-dependent running of the SNA parameters (j_1, j_2, h_1, h_2) in terms of the running of the CAR model parameters (r_u, r_v, λ, f).

C. Renormalization of the stochastic CAR model

To study the effect of external noise on chemical pathways, we add noise terms $\eta_v(t)$, $\eta_u(t)$ to the deterministic equations (5) and (6). For illustrative purposes, we choose a noise that is widespread in nature, namely power-law noise [33,34] obeying the following statistics (in Fourier space):

$$\langle \eta_v(\omega)\eta_v(\omega')\rangle = 2A_v|\omega/\omega_v|^{-\theta_v}(2\pi)\delta(\omega+\omega'), \tag{12}$$

$$\langle \eta_u(\omega)\eta_u(\omega')\rangle = 2A_u|\omega/\omega_u|^{-\theta_u}(2\pi)\delta(\omega+\omega'), \tag{13}$$

with all other moments zero. The amplitudes A_v, A_u, exponents θ_v, θ_u, and inverse timescales ω_v, ω_u are free parameters of the noise that can be adjusted experimentally. Note that other types of experimentally adjustable noise could also be envisaged.

The addition of fluctuations to the CAR model translates into a nontrivial scaling (or "running") of its parameters. The renormalization group allows us to compute this nontrivial scaling (see for example Refs. [35,36] for the application of RG to stochastic processes). Note that the exponents θ_v, θ_u are fixed by external experimental conditions, leading to loop integrals with various divergence structures. Thus caution must be exercised when applying dimensional regularization to loop integrals involving power-law noise terms with arbitrary power-law exponents. Here we follow the program developed in Refs. [25–27] to compute the running of the stochastic CAR model's parameters with scale.

For the purpose of illustration, we focus on the regime where $-3/2 < \theta_{u,v} \leqslant -1$. In this regime, and at one-loop order, only r_u and r_v develop a logarithmic divergence and run with scale. Details of the computation are shown in Appendices B–D. The result for $r_u(T)$ is [a similar but more complicated expression for $r_v(T)$ can be found in Appendix D]

$$r_u(T) = \left[r_u(T^*) + \frac{4\lambda A_v K_1}{|\delta|\omega_v^{-\theta_v}}\right]\left(\frac{T}{T^*}\right)^{|\delta|} - \frac{4\lambda A_v K_1}{|\delta|\omega_v^{-\theta_v}}, \tag{14}$$

where $K_1 = 1/[(4\pi)^{(\theta_v+2)/2}\Gamma((\theta_v+2)/2)]$, δ is the distance from the logarithmic pole, and $r_u(T^*)$ is a known value of the decay rate at some reference temporal scale T^*.

The RG analysis allows us to make the following points. The deterministic CAR model (5) and (6) exhibits various behaviors (stable solutions, oscillatory solutions, etc. [29,37,38]) depending on the values of its parameters (r_u, r_v, λ, f). Adding noise alters the behavior of the deterministic CAR model, and the renormalization group allows us to assess quantitatively the extent of this change (provided perturbation theory is valid, and that no "new chemistry" is encountered as the temporal scale T is varied [39]). In practice, adding noise to the CAR model makes its reaction rate and decay constants dependent on the noise parameters $(A_u, A_v, \theta_u, \theta_v, \omega_u, \omega_v)$ and the temporal scale T. In other words, noise converts the deterministic CAR model into an *effective* deterministic CAR model, with noise and scale dependent parameters [40].

Note that the RG here is run from a large temporal scale T^* to smaller temporal scales $T \leqslant T^*$. The running of model parameters can be controlled experimentally with the noise in the following way. We first set the noise parameters $(A_v, A_u, \theta_v, \theta_u)$ to certain values, and choose a large frequency scale $\omega_v^* = 2\pi/T^*$. The values of the model parameters (r_u, r_v, λ, f) for these values of the noise parameters are the starting point of the running in Fig. 2(a). By experimentally changing the noise parameter ω_v^* to a different value $\omega_v > \omega_v^*$, the number of frequency modes contributing to the second-order moment in Eq. (12) changes. This effectively implements the running in Fig. 2(a), going toward smaller values of $T = 2\pi/\omega_v$.

III. RESULTS AND DISCUSSION

Typically model parameters (r_u, r_v, λ, f) are not directly observable. To make contact with experiments (which is the primary goal of this paper), we apply SNA to this effective deterministic model, in order to see how noise affects observable chemical pathways and the fluxes that traverse them. To do that, we invert Eq. (11) in order to express the SNA parameters (j_1, j_2, h_1, h_2) in terms of the CAR model parameters (r_u, r_v, λ, f):

$$j_1 = \frac{f - \sqrt{f^2 - \frac{4r_u r_v^2}{\lambda}}}{2}, \quad j_2 = \frac{f + \sqrt{f^2 - \frac{4r_u r_v^2}{\lambda}}}{2}, \tag{15}$$

$$h_1 = \frac{2r_u}{f - \sqrt{f^2 - \frac{4r_u r_v^2}{\lambda}}}, \quad h_2 = \frac{2r_v}{f + \sqrt{f^2 - \frac{4r_u r_v^2}{\lambda}}}. \tag{16}$$

The sign choice follows from a stability analysis of the steady-state configurations in the CAR model, which imposes the condition $j_1 < j_2$ (see Appendix E for details).

To obtain the running of the convex parameters (j_1, j_2) and the inverse stationary concentrations (h_1, h_2) as a function of ω_v, we substitute Eqs. (14) into Eqs. (15) and (16) (note that at one-loop order and for $-3/2 < \theta_v \leqslant -1$, the reaction rate λ and the feed rate f do not run; see Appendix C). Some representative plots are shown in Fig. 2.

The decay rates (r_v, r_u) for V and U run as a function of ω_v, as shown in Fig. 2(a). As the noise frequency scale ω_v is increased, r_v increases whereas r_u decreases with respect to their values $r_u(\omega_v^*)$ and $r_v(\omega_v^*)$ measured at some reference frequency scale. Thus, from the point of view of an effective deterministic CAR model, the "nutrient" species U tends to survive longer but the replicating species V tends to decay now more rapidly. Thus the behavior of the chemical system (dictated by its parameters) depends on the characteristic frequency scale ω_v of the noise. This scale dependence is absent in the absence of external noise.

The running in the decay constants (r_v, r_u) implies a running in the convex parameters (j_1, j_2) as shown in Fig. 2(b).

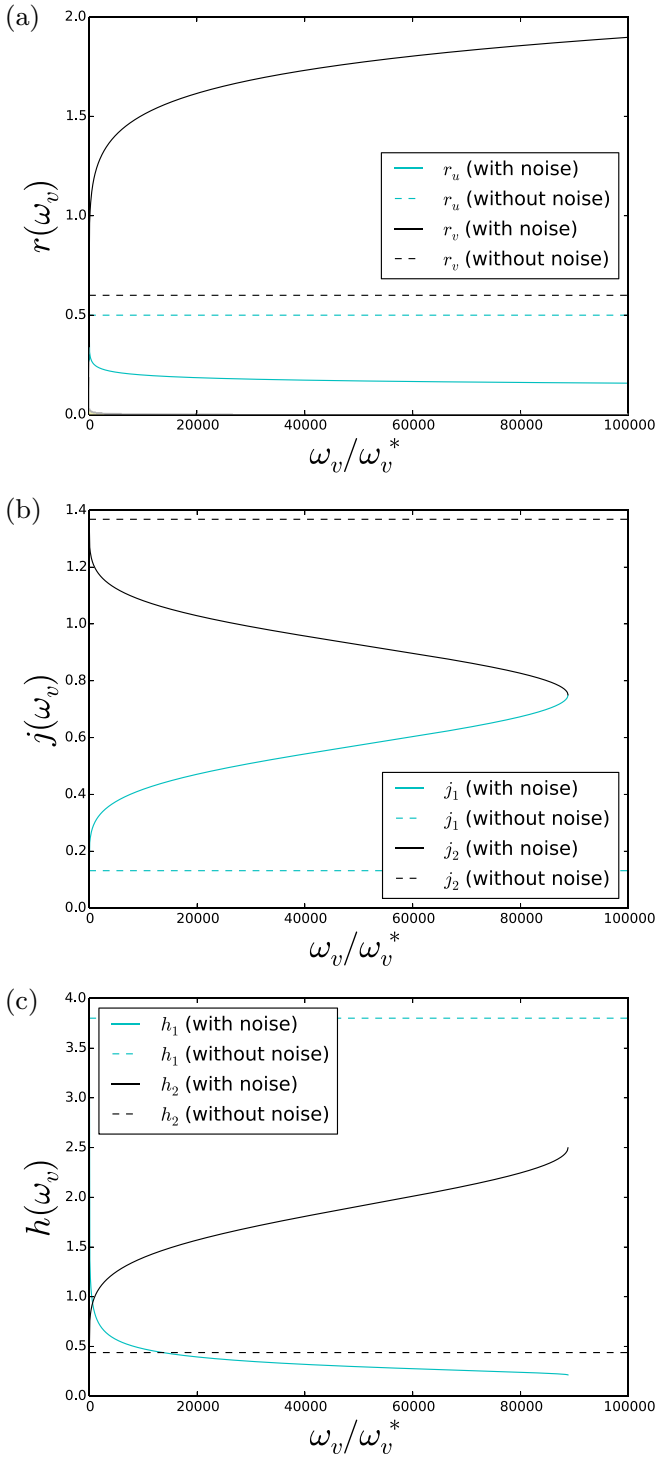

FIG. 2. Running of the parameters r_u, r_v (a), j_1, j_2 (b), and h_1, h_2 (c) as a function of scale. Fixed parameters are $\omega_v^* = 0.1$, $r_u(T^*) = 0.5$, $r_v(T^*) = 0.6$, $\lambda = 1.0$, $f = 1.5$, $\delta = 0.1$. Dotted lines represent the running without noise ($A_v = 0$, trivial scaling), while full lines represent the running with noise ($A_v = 0.001 \neq 0$).

We see that j_2 decreases and j_1 increases as ω_v increases. Thus according to Eq. (9), the matter flux traversing the catalytic pathway $\boldsymbol{E}_2$ diminishes whereas the flux through the "unproductive" pathway $\boldsymbol{E}_1$ increases as the noise frequency scale is increased. From the point of view of an observer outside the enclosing box in Fig. 1, increasing ω_v would result in a decrease of P with respect to Q.

There is a critical scale ω_v^c at which the two effective fluxes equalize $j_1(\omega_v^c) = j_2(\omega_v^c)$ and above which they are undefined. This feature follows from the relationships (15) and (16) which develop imaginary parts whenever $f^2 < \frac{4r_u r_v}{\lambda}$. If the effective decay rates at large frequency scales grow in magnitude such that they overwhelm the feed term f at or above that scale, then the latter is unable to maintain the system in a steady state, and so the SNA approach no longer applies (SNA is only valid for stationary states). In other words, the two nontrivial fixed points of Eqs. (5) and (6) (which are equal to $1/h_1$ and $1/h_2$) become complex when $f^2 < \frac{4r_u r_v}{\lambda}$ and thus do not correspond to any real concentrations for which the system is stationary. This signals the onset of a chemical instability, where the system goes from a bistable regime where the system is either "alive" ($V \neq 0$) or "dead" ($V = 0$) to a single stable regime where the system consists solely of a uniform distribution of nutrient U.

The inverse stationary state concentrations (h_1, h_2) also run with the noise frequency scale ω_v as shown in Fig. 2(c). Note here that as ω_v is increased, the observed decrease in $h_1 = 1/[V]_{ss}$ corresponds to an increase in the steady-state concentration of species V. So there is relatively more V (replicating species) at shorter timescales (greater concentrations) with respect to the concentration at the reference frequency scale ω_v^*. At the scale where the two inverse concentrations become imaginary, the system goes from a bistable to a monostable regime and effectively "dies." In this case, from the point of view of an observer outside the enclosing box in Fig. 1, decreasing the noise frequency scale ω_v would result in an increase of P with respect to Q.

IV. CONCLUSIONS

We have demonstrated that external adjustable noise can be used to control the directly observable matter fluxes that traverse the reaction pathways in an overall reaction model by combining the renormalization group with stoichiometric network analysis. For the case of the CAR model treated here, the fluxes along the driven autocatalytic pathway $\boldsymbol{E}_2$ and along the driven unproductive flow-through pathway $\boldsymbol{E}_1$ can be controlled. SNA predicts generally that the renormalization of reaction model parameters implies an associated renormalization of the convex parameters (the flux magnitudes) and the inverse stationary concentrations. The feasibility of noise-controlled fluxes is thus expected in general complex reaction networks coupled to external noise sources, and has recently been reported for the BZ reaction [9].

The physicochemical interpretation of the results of this paper opens the door to the extension and application in many directions where optimization or selection of "chemical" pathways is naturally occurring or desirable (as an example, noise control could be used to implement chemical logic gates using the approach in Ref. [41]). This is due to the fact that, depending on noise statistics, one can channel energy at the molecular levels to processes where the external energy selectively provided by the noise makes the system visit some pathways more frequently than others, as opposed to the situation without noise. A future direction for this research

would be to try this technique in more complicated chemical models, where it might be possible to shut down a pathway or activate a previously nonaccessible one. This is a direct consequence of the connection shown here between noise parameters and stoichiometry. Potential practical applications range from electrochemistry, systems chemistry, epidemiology, immunology, and ecology to large-scale industrial processes and environmental applications.

ACKNOWLEDGMENTS

J.-S.G. and J.P.-M. thank Repsol S. A. for its support, and D.H. acknowledges Project No. CTQ2017-87864-C2-2-P (MINECO), Spain.

APPENDIX A: STOICHIOMETRIC NETWORK ANALYSIS

We summarize the basic notions of the stoichiometric network analysis needed in the present paper. A fuller detailed account of SNA and a concise review are given in Refs. [19,20]. The chemical reactions for r reactions and n reacting species obeying mass-action kinetics can be written as

$$\alpha_{1j}S_1 + \cdots + \alpha_{nj}S_n \xrightarrow{k_j} \beta_{1j}S_1 + \cdots + \beta_{nj}S_n, \quad j = 1, \ldots, r, \tag{A1}$$

where the S_i, $1 \leqslant i \leqslant n$, are the chemical species and each k_j the reaction rate constant for the jth reaction. From the coefficients in Eq. (A1) we construct the $n \times r$ stoichiometric matrix $\boldsymbol{S}$ with elements:

$$S_{ij} = \beta_{ij} - \alpha_{ij}. \tag{A2}$$

The reaction rate of the jth reaction, assuming mass action kinetics, takes the form of a monomial:

$$v_j(x, k_j) = k_j \prod_{i=1}^{n} x_i^{\kappa_{ij}}, \tag{A3}$$

where $\kappa_{ij} = \alpha_{ij}$ is the molecularity of the species S_i in the jth reaction, $\boldsymbol{\kappa}$ the $n \times r$ kinetic matrix. The $x_i = [S_i]$ denote concentrations and v_j is the flux or reaction rate of the jth reaction.

Dynamic mass balance equations for the system shown in Eq. (A1) can be written as (in vector notation)

$$\frac{d\boldsymbol{x}}{dt} = \boldsymbol{S}\boldsymbol{v}. \tag{A4}$$

Just as for the stoichiometry, the pathway structure should be an invariant property of the reaction network. We can find this from the steady-state condition:

$$\boldsymbol{0} = \boldsymbol{S}\boldsymbol{v}, \tag{A5}$$

which defines the right null space of $\boldsymbol{S}$, and corresponds to the set of all stationary-state (ss) solutions ($\boldsymbol{v}$) of Eq. (A4). Since the reaction rates in Eq. (A3) are positive-definite, they satisfy $v_i(x, k) > 0$, and therefore must belong to the *intersection* of the null space Eq. (A5) with the positive orthant R_+^r:

$$v(x_{ss}, k) \in \{z \in R^r | Sz = 0, z \in R_+^r\} = \ker(S) \bigcap R_+^r. \tag{A6}$$

This intersection defines a convex polyhedral cone C_v [22] spanned by a set of M minimal generating vectors $\boldsymbol{E}_i$'s

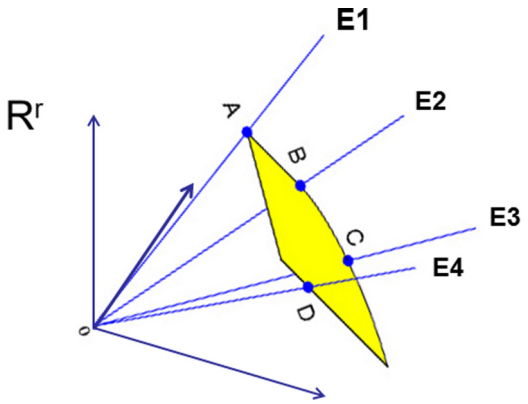

FIG. 3. The convex cone C_v, where each orthogonal axis in the positive orthant R_+^r corresponds to one of the $1 \leqslant j \leqslant r$ *stationary* reaction rates v_j [see Eq. (A3)] and so satisfies Eq. (A5) and belongs to the intersection Eq. (A6). The general stationary reaction rate can be written in vector form, as a point in this cone: a linear combination of the M cone edge vectors $\boldsymbol{E}_i$ with positive coefficients $j_i > 0$. For purposes of clarity, only four such edge vectors are drawn here.

(see Fig. 3):

$$C_v = \left\{ \boldsymbol{v} = \sum_{i=1}^{M} j_i \boldsymbol{E}_i : j_i > 0 \right\}. \tag{A7}$$

These extreme currents or extreme flux modes (EFMs) $\{\boldsymbol{E}_i\}_{i=1}^{M}$ are vectors having r components, equal to the number of reactions [20]. The positive-definite expansion coefficients $j_i > 0$ are called the convex parameters. Programs, such as COPASI, are freely available for calculating these extreme currents [42].

Define $h_i = 1/(x_{ss})_i$ as the inverse of the stationary-state concentration. Then conventional reaction rate constants can be written in terms of the SNA variables (j, h) through the identities [20]

$$k_l = \left(\sum_{i=1}^{M} j_i \boldsymbol{E}_i \right) \prod_{l} \prod_{i=1}^{n} (h_i)^{\kappa_{il}} \quad \Rightarrow \quad k_l = k_l(j, h). \tag{A8}$$

This follows immediately from Eqs. (A3) and (A7) and the definition of h_i. This general relation relates running in the reaction rate constants (k) to running in the SNA variables (j, h).

APPENDIX B: FEYNMAN RULES FOR THE CAR MODEL

Following standard procedures [23,25,35], the Feynman rules for the CAR model can be obtained from the formal solution of the CAR evolution equations. The various building blocks are shown graphically in Fig. 4, where the free response functions are given by

$$G_{u0}(\omega) = \frac{1}{-i\omega + r_u}, \tag{B1}$$

$$G_{v0}(\omega) = \frac{1}{-i\omega + r_v}, \tag{B2}$$

the noise insertions by

$$N_{u0}(\omega) = 2A_u |\omega/\omega_u|^{-\theta_u}, \tag{B3}$$

$$N_{v0}(\omega) = 2A_v |\omega/\omega_v|^{-\theta_v}, \tag{B4}$$

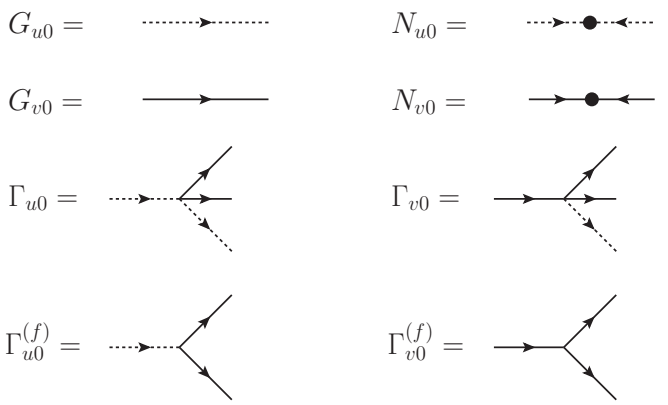

FIG. 4. Feynman rules for the CAR model. See text for definitions of symbols.

and the vertices by

$$\Gamma_{u0} = -\Gamma_{v0} = -\lambda, \tag{B5}$$

$$\Gamma^{(f)}_{u0} = -\Gamma^{(f)}_{v0} = -\frac{\lambda f}{r_u}. \tag{B6}$$

To write down a specific Feynman diagram, the above graphical rules must be supplemented with conservation of frequency at each vertex and integration over undetermined frequencies. Note that to obtain the vertices in Eq. (B6), we use the redefinition $U \to \tilde{U} = U - f/r_u$ to get rid of the constant feeding term.

APPENDIX C: POWER COUNTING

In this paper, we restrict ourselves to one-loop calculations, and we are interested in diagrams that diverge in the ultraviolet (UV). For power counting purposes, response functions and noise insertions can be estimated as follows in the UV limit:

$$G_{v0} \sim G_{u0} \sim \omega^{-1}, \tag{C1}$$

$$N_{v0} \sim N_{u0} \sim A_{u,v}\omega^{-\theta_{u,v}}, \tag{C2}$$

and each loop integration contributes one power of ω. Using the above, we can find the UV divergence structure of corrections to various CAR model parameters.

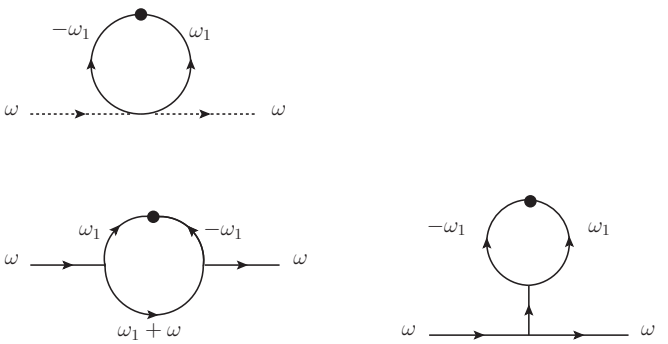

FIG. 5. One-loop corrections to G_{u0} (top row) and G_{v0} (lower row).

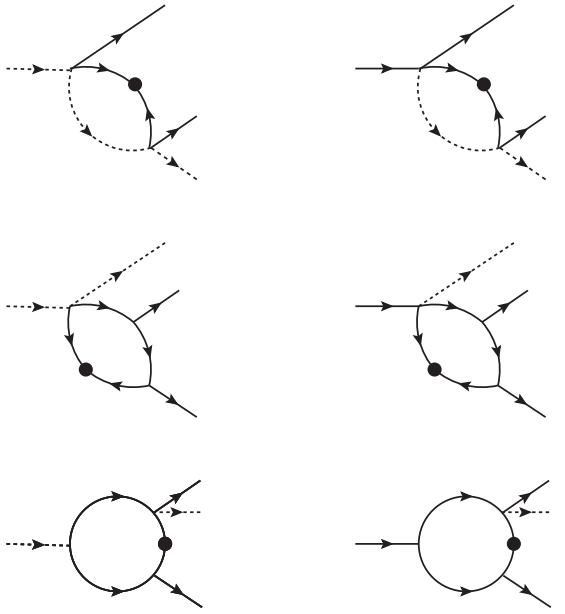

FIG. 6. One-loop corrections to Γ_{u0} (left column) and Γ_{v0} (right column).

Figure 5 shows one-loop diagrams corresponding to corrections to G_{u0} and G_{v0} (or r_u and r_v). Power counting gives $\Gamma^{(\text{row 1})}_{r_u} \sim \Gamma^{(\text{row 2,right})}_{r_v} \sim \Lambda^{-\theta_v-1}$ and $\Gamma^{(\text{row 2,left})}_{r_v} \sim \Lambda^{-\theta_v-2}$, where Λ is a large frequency cutoff scale. One-loop corrections to Γ_{u0} and Γ_{v0} (or λ) are shown in Fig. 6. Counting powers of frequency for each diagram, we get that $\Gamma^{(\text{row 1})}_{u} \sim -\Gamma^{(\text{row 1})}_{v} \sim \Lambda^{-\theta_v-2}$ and $\Gamma^{(\text{row 2})}_{u} \sim -\Gamma^{(\text{row 2})}_{v} \sim \Gamma^{(\text{row 3})}_{u} \sim -\Gamma^{(\text{row 3})}_{v} \sim \Lambda^{-\theta_v-3}$. One-loop corrections to $\Gamma^{(f)}_{u0}$ and $\Gamma^{(f)}_{v0}$ (or f) are shown in Fig. 7. Power counting gives $\Gamma^{(f)\,(\text{row 1})}_{u} \sim -\Gamma^{(f)\,(\text{row 1})}_{v} \sim \Lambda^{-\theta_v-2}$ and $\Gamma^{(f)\,(\text{row 2})}_{u} \sim -\Gamma^{(f)\,(\text{row 2})}_{v} \sim \Lambda^{-\theta_v-3}$. One-loop corrections to N_{u0} and N_{v0} (or A_u and A_v) are shown in Fig. 8. Counting powers of frequency for each diagram, we get that $N_u \sim N_v \sim \Lambda^{-2\theta_v-3}$.

Note that none of the one-loop diagrams shown in Figs. 5–8 depend on the noise $\eta_u(t)$. Noise on the U chemical starts to contribute to the running of parameters at two-loop, and

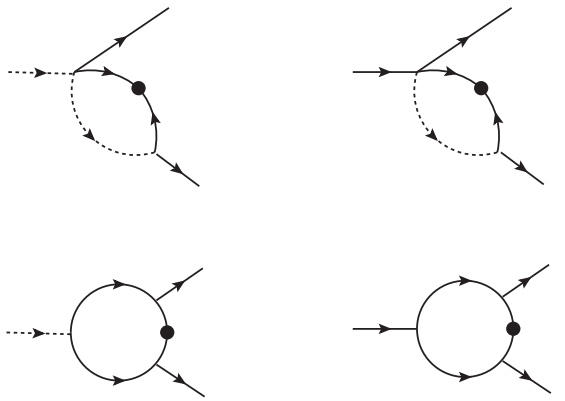

FIG. 7. One-loop corrections to $\Gamma^{(f)}_{u0}$ (left column) and $\Gamma^{(f)}_{v0}$ (right column).

FIG. 8. One-loop corrections to N_{v0} (left column) and N_{u0} (right column).

is thus negligible compared to the effect of noise on the V chemical.

Each diagram in Figs. 5–8 may be UV divergent, depending on the noise exponent θ_v. From the above power counting, we can identify three regimes:

Regime 1. When $-\frac{3}{2} < \theta_v \leqslant -1$, two parameters ($r_u$ and r_v) run.

Regime 2. When the temporal noise exponent is $-2 < \theta_v \leqslant -\frac{3}{2}$, four parameters ($r_u, r_v, A_u, A_v$) run. There is even a chance that the exponents themselves (θ_u, θ_v) might also run, depending on the form of the one-loop corrections.

Regime 3. When the temporal noise exponent is $\theta_v \leqslant -2$, six parameters ($r_u, r_v, A_u, A_v, \lambda, f$) run. For low enough values of θ_v, non-renormalizable operators might also play an important role in the dynamics, as discussed in Ref. [25].

For simplicity and for the purpose of illustration, we concentrate on regime 1 in the following.

APPENDIX D: RENORMALIZATION GROUP FLOW OF THE MODEL PARAMETERS

In this section, we present some details on how to obtain the running of the model parameter r_u (r_v is done in a similar way) by computing its β function. We start with the one-loop correction to the response function G_{u0} (see Fig. 5, top row):

$$\begin{aligned}\Gamma_{r_u}(\omega') &= -\frac{2\lambda A_v}{\omega_v^{-\theta_v}} \int \frac{d\omega}{(2\pi)} \, |\omega|^{-\theta_v} \, G_{v0}(\omega) G_{v0}(-\omega) \\ &= -\frac{2\lambda A_v}{\omega_v^{-\theta_v}} \int \frac{d\omega}{(2\pi)} \, |\omega|^{-\theta_v} \left(\frac{1}{\omega^2 + r_v^2}\right). \end{aligned} \tag{D1}$$

To regulate this potentially divergent integral, we analytically continue the time dimension to z:

$$\Gamma_{r_u}(\omega') = -\frac{2\lambda A_v^{(z)}}{\omega_v^{-\theta_v}} \int \frac{d^z\omega}{(2\pi)^z} \, |\omega|^{-\theta_v} \left(\frac{1}{\omega^2 + r_v^2}\right), \tag{D2}$$

where the superscript (z) in $A_v^{(z)}$ indicates that the engineering dimension of the noise amplitude depends on the analytically continued time dimension z. The integral in Eq. (D2) can be done using the method regularization in the presence of noise of Ref. [26]. The result is

$$\Gamma_{r_u}(\omega') = -\frac{2\lambda A_v^{(z)}}{\omega_v^{-\theta_v}} \frac{\pi}{(4\pi)^{z/2}\Gamma(z/2)} \frac{(r_v)^{-2+z-\theta_v}}{\sin \pi\left(\frac{z}{2} - \frac{\theta_v}{2}\right)}. \tag{D3}$$

Equation (D3) has an infinite number of poles, and the locations of those poles depend on the noise exponent θ_v. Focusing on regime 1, we expand Eq. (D3) around the pole located at $\theta_v = -1$, corresponding to a logarithmic UV divergence. Defining the quantity $z - \theta_v = 2 - \delta$ for convenience and performing a δ expansion of Eq. (D3), we obtain

$$\Gamma_{r_u}(\omega') = -\frac{4\lambda A_v^{(\theta_v+2)} K_1}{\omega_v^{-\theta_v}} \frac{1}{\delta} + \text{finite}, \tag{D4}$$

where $K_1 = 1/[(4\pi)^{(\theta_v+2)/2}\Gamma((\theta_v+2)/2)]$ and "finite" means terms that are finite in the $\delta \to 0$ limit. Those terms are not necessary for β-function computations, and we ignore them in the following.

The Z factor for r_u is given by

$$Z_{r_u} = 1 + \frac{\Gamma_{r_u}(\omega')}{r_u} = 1 - \frac{4 g_u^{(z)} K_1 T^\delta}{\delta}, \tag{D5}$$

where T is an arbitrary temporal scale and where we defined the effective coupling:

$$g_u^{(z)} = \frac{\lambda A_v^{(z)}}{r_u}. \tag{D6}$$

The β function for r_u is obtained by taking the derivative of the bare effective coupling (D6) with respect to the arbitrary timescale T. The result is

$$\beta_{g_u} \equiv T \frac{dg_u}{dT} = \delta g_u - 4 g_u^2 K_1 + O(g^3). \tag{D7}$$

In terms of the original model parameters, the β function becomes

$$\beta_{r_u} \equiv T \frac{dr_u}{dT} = -\delta r_u + \frac{4\lambda A_v K_1}{\omega_v^{-\theta_v}}. \tag{D8}$$

Integrating the above β function gives the running of r_u as a function of the arbitrary temporal scale T:

$$r_u(T) = \left[r_u(T^*) + \frac{4\lambda A_v K_1}{|\delta|\omega_v^{-\theta_v}}\right]\left(\frac{T}{T^*}\right)^{|\delta|} - \frac{4\lambda A_v K_1}{|\delta|\omega_v^{-\theta_v}}, \tag{D9}$$

where $r_u(T^*)$ is an experimentally known value of the decay rates at some reference temporal scale T^*. The expression for $r_v(T)$ can be obtained in a similar way:

$$\begin{aligned} r_v(T) = \left(\frac{T}{T^*}\right)^{-|\delta|} \Bigg[& r_v^2(T^*) + \frac{\frac{16\lambda^2 f^2 A_v K_1}{|\delta|\omega_0^{-\theta_v}} \ln\left(\frac{r_u(T^*)}{r_u(T)}\right)}{\left[r_u(T^*) + \frac{4\lambda A_v K_1}{|\delta|\omega_0^{-\theta_v}}\right]^2} \\ & - \frac{\frac{64\lambda^3 f^2 A_v^2 K_1^2}{|\delta|^2\omega_0^{-2\theta_v}}\left(\frac{1}{r_u(T^*)} - \frac{1}{r_u(T)}\right)}{\left[r_u(T^*) + \frac{4\lambda A_v K_1}{|\delta|\omega_0^{-\theta_v}}\right]^2} \Bigg]^{1/2}. \end{aligned} \tag{D10}$$

APPENDIX E: STABILITY ANALYSIS OF STEADY STATES

Stability analysis is carried out in terms of the positive convex parameters $j_i > 0$ and the positive inverse stationary concentrations $h_i > 0$. The Jacobian matrix is given by [43]

$$\mathrm{Jac}(\boldsymbol{j}, \boldsymbol{h}) = \boldsymbol{S}\mathrm{diag}(\boldsymbol{j} \cdot \boldsymbol{E})\boldsymbol{\kappa}^{\boldsymbol{T}}\mathrm{diag}(\boldsymbol{h}). \tag{E1}$$

Substituting in Eqs. (7) and (8) this gives

$$\mathrm{Jac}(\boldsymbol{j}, \boldsymbol{h}) = \begin{pmatrix} -h_1(j_1 + j_2) & -2h_2 j_2 \\ h_1 j_2 & h_2 j_2 \end{pmatrix}, \tag{E2}$$

and its characteristic polynomial $P(\lambda) = \lambda^2 + a_1\lambda + a_2$, where $a_1 = -h_2 j_2 + h_1(j_1 + j_2)$, and $a_2 = h_1 h_2 j_2 (j_2 - j_1)$. Then the stability of the stationary states $h_1 > 0, h_2 > 0$ requires that both coefficients $a_1 > 0$ and $a_2 > 0$ be positive simultaneously [44]. This leads to

$$j_2 > j_1 \quad \text{and} \quad \frac{j_1 + j_2}{j_2} > \frac{h_2}{h_1} > 0 \tag{E3}$$

as claimed.

[1] M. E. Peskin and D. V. Schroeder, *An Introduction to Quantum Field Theory* (Perseus Books Publishing, Cambridge, 1995).

[2] J. Zinn-Justin, *Quantum Field Theory and Critical Phenomena* (Oxford University Press, Oxford, 2002).

[3] J. Garcia-Ojalvo and J. M. Sancho, *Noise in Spatially Extended Systems* (Springer, New York, 1999).

[4] W. Horsthemke and R. Lefever, *Noise-Induced Transitions* (Springer, Berlin, 2006).

[5] J. M. A. Carnall, C. A. Waudby, A. M. Belenguer, M. C. A. Stuart, J. J. P. Peyralans, and S. Otto, Science **327**, 1502 (2010).

[6] D. S. A. Simakov and J. Pérez-Mercader, J. Phys. Chem. A **117**, 13999 (2013).

[7] D. S. A. Simakov and J. Pérez-Mercader, Sci. Rep. **3**, 2404 (2013).

[8] Z. Hou and H. Xin, Phys. Rev. E **60**, 6329 (1999).

[9] R. Srivastava, M. Dueñas-Díez, and J. Pérez-Mercader, React. Chem. Eng. **3**, 216 (2018).

[10] F. Lesmes, D. Hochberg, F. Morán, and J. Pérez-Mercader, Phys. Rev. Lett. **91**, 238301 (2003).

[11] T. Biancalani, F. Jafarpour, and N. Goldenfeld, Phys. Rev. Lett. **118**, 018101 (2017).

[12] J. García-Ojalvo and L. Schimansky-Geier, Europhys. Lett. **47**, 298 (1999).

[13] I. Sendiña-Nadal, S. Alonso, V. Pérez-Muñuzuri, M. Gómez-Gesteira, V. Pérez-Villar, L. Ramírez-Piscina, J. Casademunt, J. M. Sancho, and F. Sagués, Phys. Rev. Lett. **84**, 2734 (2000).

[14] L. Q. Zhou, X. Jia, and Q. Ouyang, Phys. Rev. Lett. **88**, 138301 (2002).

[15] B. Lindner, J. García-Ojalvo, A. Neiman, and L. Schimansky-Geier, Phys. Rep. **392**, 321 (2004).

[16] For systems with a low number of constituents, both external noise (e.g., temperature, luminosity, and stirring) and internal noise (quantum mechanical randomness) may affect the dynamic of the chemical system. The treatment of internal noise requires more refined tools than the one used in this paper, as discussed in the review [45]. See also Refs. [46,47] for a study of internal noise in the CAR model.

[17] Note that due to the external energy provided by the noise, this selection of chemical pathways may include pathways previously inaccessible to the system. Although this behavior is not present in the simple cubic autocatalytic reaction used to illustrate our method, there is no theoretical constraint that precludes this in a more complex chemical system.

[18] A. K. Horváth, M. Dolnik, A. P. Muñuzuri, A. M. Zhabotinsky, and I. R. Epstein, Phys. Rev. Lett. **83**, 2950 (1999).

[19] B. L. Clarke, in *Advances in Chemical Physics*, edited by I. Prigogine and S. A. Rice (John Wiley, 1980), Vol. 43, pp. 1–215.

[20] B. L. Clarke, Cell Biophys. **12**, 237 (1988).

[21] B. L. Clarke, J. Chem. Phys. **75**, 4970 (1981).

[22] R. T. Rockafeller, *Convex Analysis* (Princeton University Press, Princeton, 1970).

[23] D. Hochberg, F. Lesmes, F. Morán, and J. Pérez-Mercader, Phys. Rev. E **68**, 066114 (2003).

[24] M. P. Zorzano, D. Hochberg, and F. Morán, Phys. A (Amsterdam, Neth.) **334**, 67 (2004).

[25] J. S. Gagnon and J. Pérez-Mercader, Phys. A (Amsterdam, Neth.) **480**, 51 (2017).

[26] J. S. Gagnon, D. Hochberg, and J. Pérez-Mercader, Phys. Rev. E **92**, 042114 (2015).

[27] J.-S. Gagnon, D. Hochberg, and J. Pérez-Mercader, Phys. Rev. E **95**, 032106 (2017).

[28] E. E. Sel'kov, Eur. J. Biochem. **4**, 79 (1968).

[29] P. Gray and S. K. Scott, J. Phys. Chem. **89**, 22 (1985).

[30] J. E. Pearson, Science **261**, 189 (1993).

[31] W. Mazin, K. E. Rasmussen, E. Mosekilde, P. Borckmans, and G. Dewel, Math. Comput. Simul. **40**, 371 (1996).

[32] F. Cooper, G. Ghoshal, A. Pawling, and J. Pérez-Mercader, Phys. Rev. Lett. **111**, 044101 (2013).

[33] J. Pérez-Mercader, in *Astrobiology: The Quest for the Conditions of Life*, edited by G. Horneck and C. Baumstark-Khan (Springer, Berlin, 2002), pp. 337–360.

[34] M. E. J. Newman, Contemp. Phys. **46**, 323 (2005).

[35] E. Medina, T. Hwa, M. Kardar, and Y. C. Zhang, Phys. Rev. A **39**, 3053 (1989).

[36] U. W. Täuber, *Critical Dynamics: A Field Theory Approach to Equilibrium and Non-Equilibrium Scaling Behavior* (Cambridge University Press, Cambridge, 2014).

[37] P. Gray and S. K. Scott, Chem. Eng. Sci. **38**, 29 (1983).

[38] P. Gray and S. K. Scott, Chem. Eng. Sci. **39**, 1087 (1984).

[39] If "new chemistry" comes into play at shorter temporal scales, then new species and interactions must be added to Eqs. (5) and (6). These new interactions might add corrections to the running of the parameters [cf. Eq. (14)] that are suppressed by the small temporal scale of the new chemistry [25].

[40] Since the CAR model is perturbatively renormalizable at one loop [45], adding noise to Eqs. (5) and (6) does not change the form of the original equations [48].

[41] M. Egbert, J.-S. Gagnon, and J. Pérez-Mercader, J. R. Soc., Interface **15**, 0169 (2018).

[42] S. Hoops, S. Sahle, R. Gauges, C. Lee, J. Pahle, N. Simus, M. Singhal, L. Xu, P. Mendes, and U. Kummer, Bioinformatics **22**, 3067 (2006).

[43] K. Gatermann, M. Eiswirth, and A. Sensse, J. Symb. Comput. **40**, 1361 (2005).

[44] J. D. Murray, *Mathematical Biology* (Springer-Verlag, Berlin, 1993).

[45] U. C. Taüber, M. Howard, and B. P. Vollmayr-Lee, J. Phys. A **38**, R79 (2005).

[46] D. Hochberg, M.-P. Zorzano, and F. Morán, J. Chem. Phys. **122**, 214701 (2005).

[47] F. Cooper, G. Ghoshal, and J. Pérez-Mercader, Phys. Rev. E **89**, 062127 (2014).

[48] D. Hochberg, J. Pérez-Mercader, C. Molina-Paris, and M. Visser, Int. J. Mod. Phys. A **14**, 1485 (1999).